

PSD-95 promotes synaptogenesis and multiinnervated spine formation through nitric oxide signaling

Irina Nikonenko,^{1,2} Bernadett Boda,¹ Sylvain Steen,¹ Graham Knott,^{2,3} Egbert Welker,² and Dominique Muller¹

¹Department of Fundamental Neuroscience, Geneva Neuroscience Center, University of Geneva School of Medicine, CH-1211 Geneva, Switzerland

²Département de Biologie Cellulaire et de Morphologie, Université de Lausanne, CH-1005 Lausanne, Switzerland

³Interdisciplinary Center for Electron Microscopy, Swiss Federal Institute of Technology, CH-1015 Lausanne, Switzerland

Postsynaptic density 95 (PSD-95) is an important regulator of synaptic structure and plasticity. However, its contribution to synapse formation and organization remains unclear. Using a combined electron microscopic, genetic, and pharmacological approach, we uncover a new mechanism through which PSD-95 regulates synaptogenesis. We find that PSD-95 overexpression affected spine morphology but also promoted the formation of multiinnervated spines (MISs) contacted by up to seven presynaptic terminals. The formation of multiple contacts was specifically prevented by deletion of the PDZ₂ domain of PSD-95, which interacts with nitric oxide (NO)

synthase (NOS). Similarly, PSD-95 overexpression combined with small interfering RNA-mediated down-regulation or the pharmacological blockade of NOS prevented axon differentiation into varicosities and multisynapse formation. Conversely, treatment of hippocampal slices with an NO donor or cyclic guanosine monophosphate analogue induced MISs. NOS blockade also reduced spine and synapse density in developing hippocampal cultures. These results indicate that the postsynaptic site, through an NOS-PSD-95 interaction and NO signaling, promotes synapse formation with nearby axons.

Introduction

Postsynaptic scaffolding proteins of the membrane-associated guanylate kinase family, which includes such members as postsynaptic density 95 (PSD-95), SAP-97, or SAP102, play major roles in synapse organization and function (Funke et al., 2005). Among these proteins, PSD-95 has been particularly studied because in the central nervous system it is one of the major constituents of excitatory PSDs (Chen et al., 2005), and it is directly involved in synaptic plasticity (Migaud et al., 1998). Overexpression of PSD-95 in neurons is associated with modifications in the properties of synaptic transmission, which mimic and occlude long-term potentiation (LTP; Stein et al., 2003). This effect appears to be related to a role of PSD-95 in the synaptic targeting of α -amino-3-hydroxy-5-methyl-4-isoxazolepropionic acid (AMPA) receptors (Chen et al., 2000; Schnell et al., 2002) and in their regulated expression during plasticity (Ehrlich and Malinow, 2004). For this, PSD-95 interacts with the AMPA receptor-associated protein stargazin (Schnell et al., 2002) and reg-

ulates not only the surface expression of AMPA receptors but also their diffusion and trapping at synaptic sites (Bats et al., 2007).

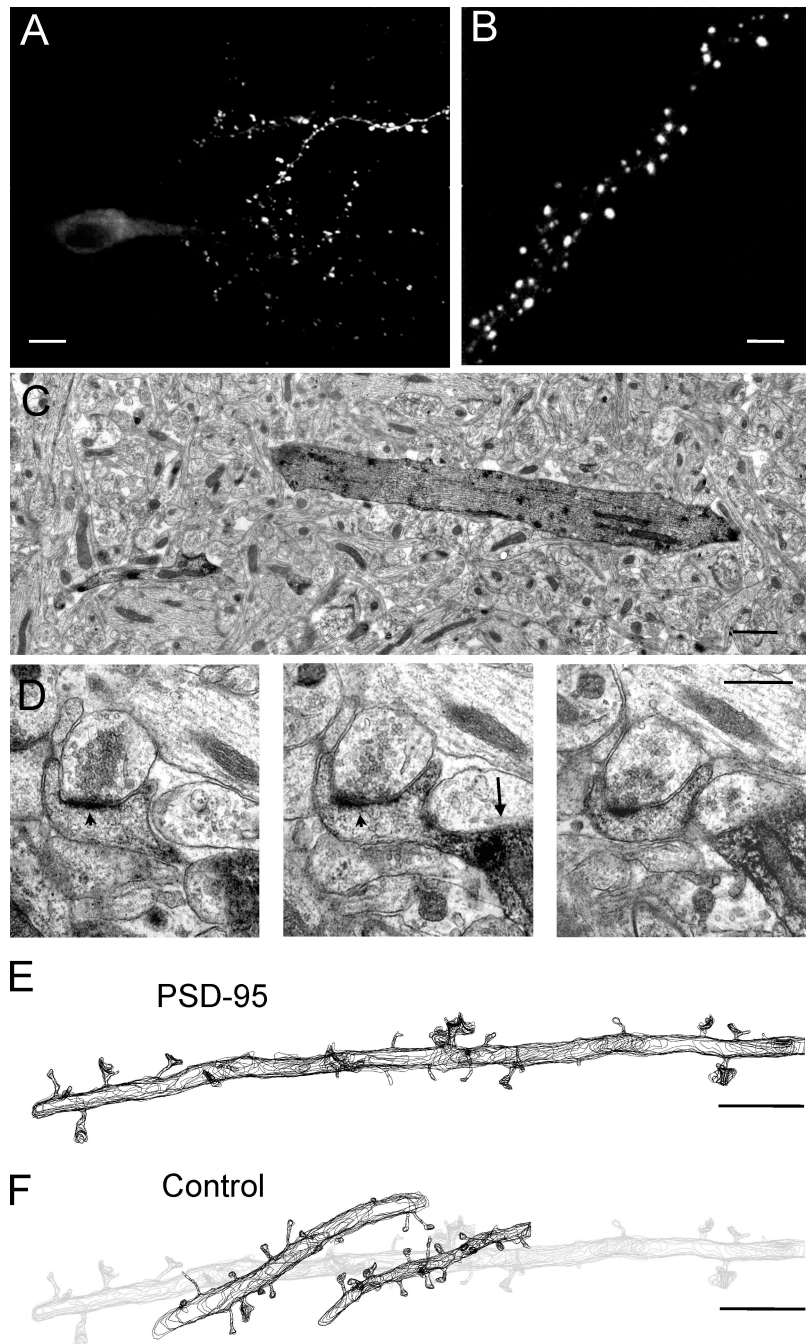
In addition to synaptic function, PSD-95 has also been proposed to affect synapse maturation and stabilization (El-Husseini et al., 2000; Ehrlich et al., 2007; De Roo et al., 2008) and, thus, synapse number. Acute knockdown of PSD-95 reduces the development of synaptic structures (Ehrlich et al., 2007), and PSD-95 mutant mice exhibit variations in spine densities in several brain regions (Vickers et al., 2006). However, these mechanisms remain essentially unexplained but could depend on several interesting properties of the protein. PSD-95 shows a continuous dynamic regulation between intracellular and synaptic pools (Bresler et al., 2001; Gray et al., 2006) and also interacts with several important synaptic proteins, including synaptic GTPase-activating protein, neuroligins, or nitric oxide (NO) synthase (NOS), which might mediate trans-synaptic signaling (Kim and Sheng, 2004) for synapse formation or stabilization.

Correspondence to Dominique Muller: Dominique.Muller@medecine.unige.ch

Abbreviations used in this paper: AMPA, α -amino-3-hydroxy-5-methyl-4-isoxazolepropionic acid; cGMP, cyclic guanosine monophosphate; DETA, diethylene-triamine; DIV, day in vitro; L-NAME, L-N^G-nitroarginine methyl ester; LTP, long-term potentiation; MIS, multiinnervated spine; nNOS, neuronal NOS; NO, nitric oxide; NOS, NO synthase; PSD, postsynaptic density.

© 2008 Nikonenko et al. This article is distributed under the terms of an Attribution-Noncommercial-Share Alike-No Mirror Sites license for the first six months after the publication date [see <http://www.jcb.org/misc/terms.shtml>]. After six months it is available under a Creative Commons License [Attribution-Noncommercial-Share Alike 3.0 Unported license, as described at <http://creativecommons.org/licenses/by-nc-sa/3.0/>].

Figure 1. PSD-95-overexpressing pyramidal neurons in hippocampal slice cultures. (A) Low magnification confocal view of a CA1 pyramidal cell 2 d after transfection with a PSD-95-EGFP construct. (B) Higher magnification of a dendritic segment illustrating the characteristic punctate aspect of PSD staining obtained after PSD-95-EGFP overexpression. (C) Low magnification electron microscopic view of a section through a dendrite (dark) of a transfected neuron upon revelation of EGFP immunostaining. (D) Higher magnification serial sections of a dendritic spine from an EGFP-immunostained neuron (the arrow points to a dendrite). Note the presence of a clearly visible PSD (arrowheads). (E) Contour representation of the multiple sections obtained from a three-dimensionally reconstructed dendritic segment of a PSD-95-EGFP-transfected cell. Note the presence of many large dendritic spines. (F) Three-dimensionally reconstructed dendritic segments (dark contours) from nontransfected neurons located in the vicinity of the PSD-95-transfected cell (light gray contours). Bars: (A) 10 μ m; (B, E, and F) 5 μ m; (C) 1 μ m; (D) 0.5 μ m.



To examine these issues, we used a quantitative electron microscopic analysis of serially sectioned dendritic segments of CA1 neurons in hippocampal slice cultures and found that overexpression of PSD-95 not only affected the morphological characteristics of dendritic spines but also resulted in the formation of spines contacted by several different presynaptic partners. Through genetic and pharmacological manipulations, we provide evidence that this effect depends on an interaction between PSD-95 and NOS and requires NO signaling. Together, these data identify a novel mechanism through which expression of PSD-95 promotes synapse formation with nearby axons, a result that strongly emphasizes the importance of the postsynaptic element in driving contact formation during synaptogenesis.

Results

Ultrastructural analyses of PSD-95-transfected pyramidal neurons

To examine the effect of PSD-95 overexpression on spine morphology, we transfected hippocampal organotypic slice cultures with a PSD-95 tagged with EGFP using a biolistic approach. 2 d after transfection, neurons showed the classical punctuate PSD-95 staining of synapses (Fig. 1, A and B). The tissue was then processed for EM analyses using anti-EGFP antibodies to reveal the transfected neurons and their dendritic spines (Fig. 1, C and D). Through serial sectioning and 3D reconstruction of labeled dendritic segments (Fig. 1 E), we examined the ultrastructural

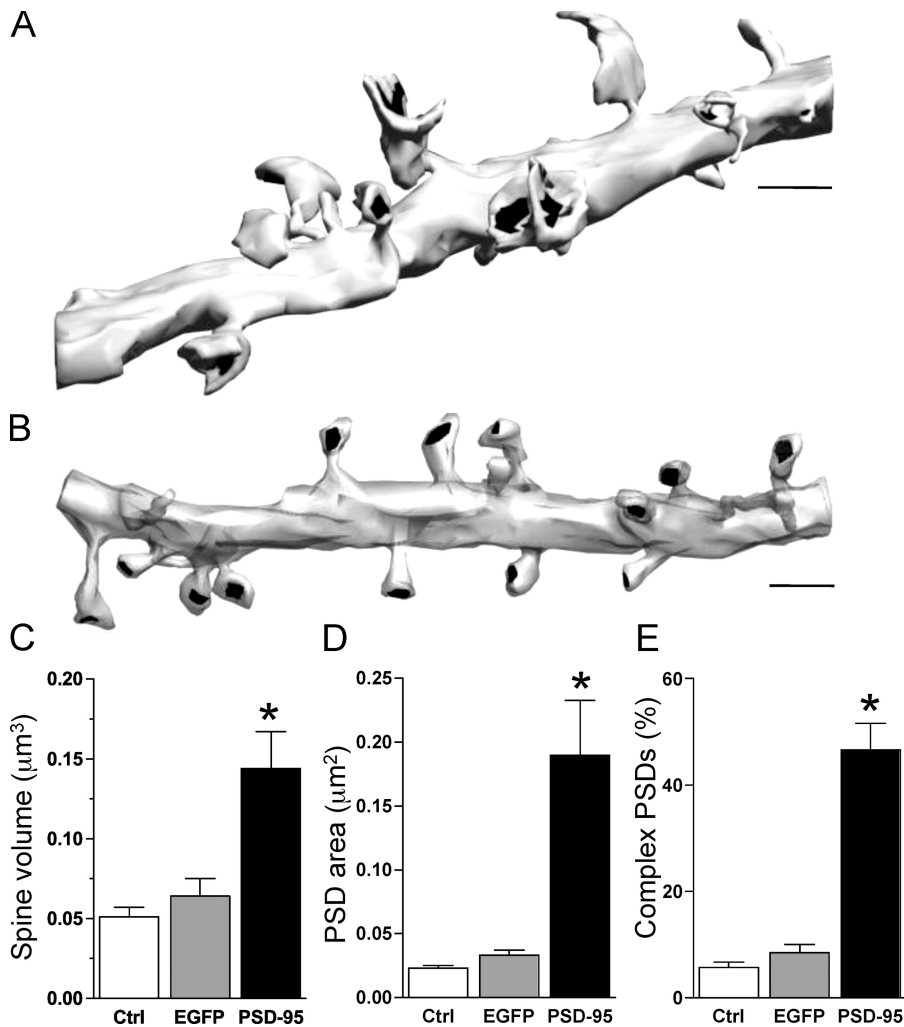


Figure 2. Spine enlargement induced by PSD-95 overexpression. (A) Three-dimensionally reconstructed dendritic segment of a PSD-95-transfected cell illustrating the presence of numerous large spines regularly exhibiting perforated PSDs. (B) Three-dimensionally reconstructed dendritic segment of a control cell. Note the smaller size of the spines. (C) Spine volume measured in control nontransfected (ctrl; $n = 8$ cells; 145 spines), EGFP-transfected ($n = 4$ cells; 164 spines), and PSD-95-transfected ($n = 7$ cells; 234 spines) pyramidal neurons. Data are mean \pm SEM (error bars; *, $P < 0.05$). (D) Same as in C but for the total PSD area. (E) Same as in C but for the proportion of spines with complex PSDs. Bars, 1 μm .

characteristics and distribution of synapses. As controls, we analyzed EGFP-transfected neurons and also nontransfected neurons located close to the PSD-95- or EGFP-transfected cells (Fig. 1 F). In total, 1,314 spine synapses from 72 different cells obtained under 12 different conditions were three-dimensionally reconstructed in this study (Table S1, available at <http://www.jcb.org/cgi/content/full/jcb.200805132/DC1>).

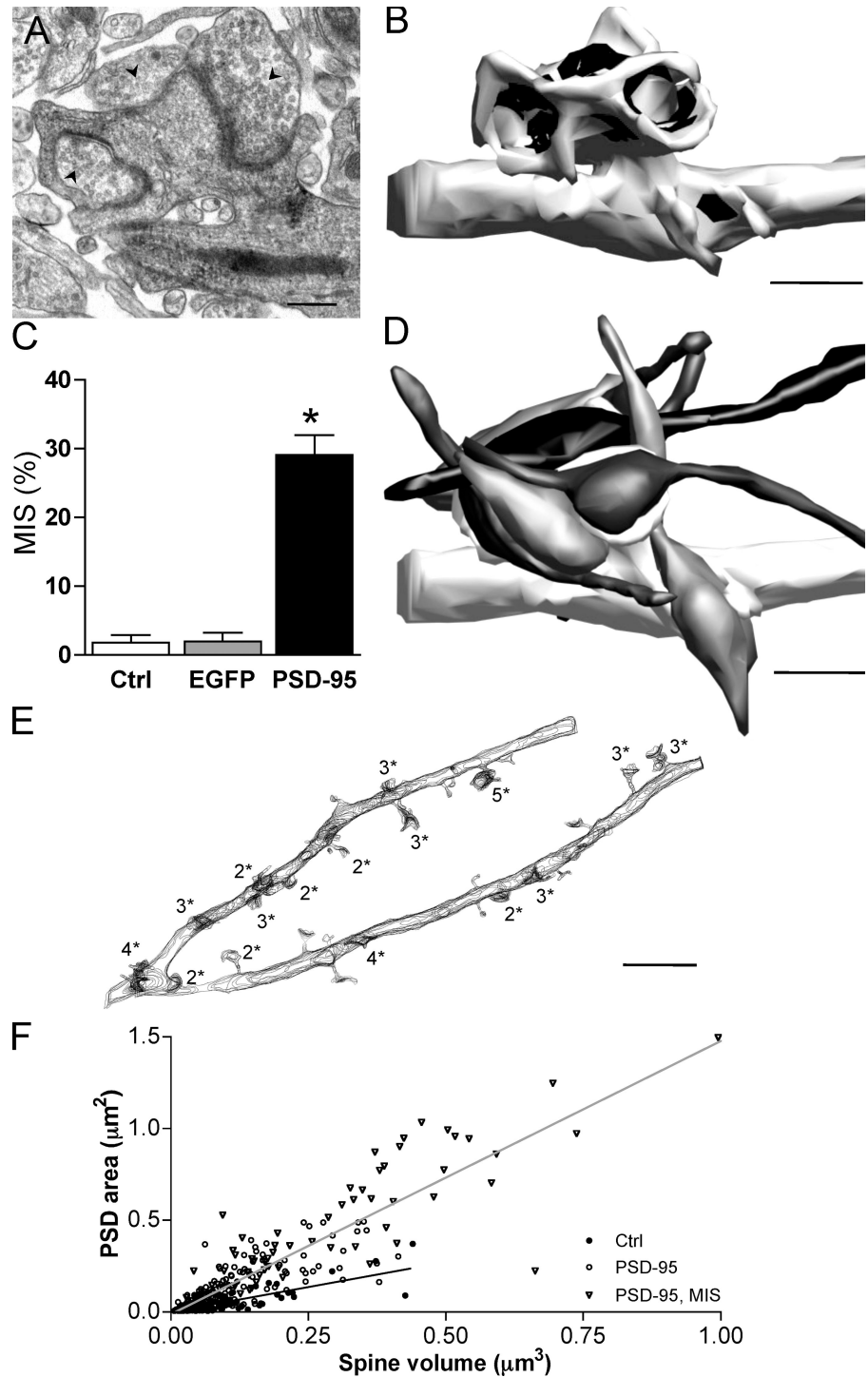
As shown in Fig. 2, PSD-95 overexpression modified the ultrastructural features of dendritic spines and PSDs. Analysis of 234 spines from PSD-95-transfected neurons ($n = 7$ cells), 164 spines from EGFP-transfected cells ($n = 4$ cells), and 145 spines from nontransfected neurons ($n = 8$ cells) showed that spines in PSD-95-transfected cells become much larger, often with complex shapes and membrane extensions that engulf presynaptic terminals. The spine volume increased by factors of 2.3 and 2.8 when compared with either EGFP neurons ($0.144 \pm 0.023 \mu\text{m}^3$ vs. $0.064 \pm 0.011 \mu\text{m}^3$) or nontransfected neurons ($0.051 \pm 0.006 \mu\text{m}^3$; $P < 0.05$; Fig. 2 C). The increase of the PSD area was even more pronounced (5.7 \times and 8.2 \times the mean value of EGFP and control neurons; $0.189 \pm 0.043 \mu\text{m}^2$ vs. $0.033 \pm 0.004 \mu\text{m}^2$ and $0.023 \pm 0.002 \mu\text{m}^2$, respectively; $P < 0.05$; Fig. 2 D). The proportion of spines with complex PSDs, characterized by a discontinuity on a single section, was also significantly in-

creased in comparison with control cells ($46.6 \pm 5\%$ vs. $8.5 \pm 1\%$ or $5.7 \pm 1.4\%$; $P < 0.05$; Fig. 2 E). In addition, PSD-95 overexpression resulted in a decrease in spine density as indicated by analysis of the three-dimensionally reconstructed segments (PSD-95, 0.63 ± 0.12 spines/ μm of dendritic length; EGFP, 0.96 ± 0.29 spines/ μm of dendritic length; $n = 7$ and 4 cells, respectively; $P < 0.05$; Table S1), a result also confirmed by analyzing the number of fluorescent puncta observed on transfected cell dendrites (PSD-95-transfected cells, 0.74 ± 0.03 puncta/ μm ; spines on EGFP-transfected cells, 0.94 ± 0.09 puncta/ μm ; $n = 14$ and 8 cells, respectively; $P < 0.05$).

Multiinnervated spines (MISs) in PSD-95-transfected cells

EM analysis of PSD-95-transfected neurons revealed the presence of numerous MISs characterized by several presynaptic terminals contacting the same postsynaptic spine through independent PSDs (Fig. 3, A, B, and D; Fig. S1, and Videos 1 and 2, available at <http://www.jcb.org/cgi/content/full/jcb.200805132/DC1>). MISs contacted by two terminals can be observed in the hippocampus in vivo and in vitro and account for a small fraction of all spines, although during the early postnatal development, dendritic protrusions exhibiting multiple synaptic contacts

Figure 3. MISs induced by PSD-95 over-expression. (A) EM picture of a section through an MIS showing three axonal terminals (arrowheads) making synaptic contacts with a transfected spine. (B) 3D reconstruction of the same MIS making synaptic contacts with six different presynaptic terminals. Axons have been omitted, and the black regions represent PSDs. (C) Proportion of MISs observed under control conditions (ctrl; $n = 8$ cells; 145 spines), in cells transfected with EGFP ($n = 4$ cells; 164 spines), and PSD-95 ($n = 7$ cells; 234 spines; *, $P < 0.05$). Data are mean \pm SEM (error bars). (D) Same as in B but including the presynaptic terminals and axons. See the animated versions in Videos 1 and 2 (available at <http://www.jcb.org/cgi/content/full/jcb.200805132/DC1>). (E) Contour representation of a dendritic segment from a PSD-95-transfected cell showing the distribution and complexity of MISs (numbers refer to presynaptic terminals [*] making synaptic contacts on the spine). (F) Graph showing the distribution of total PSD areas (sum of all PSDs on a given spine) as a function of spine volume under control conditions (closed circles), in PSD-95-transfected cells (open circles), and for MISs of PSD-95-transfected cells (triangles). The two lines indicate the linear regression obtained for control spines and for spines of PSD-95-transfected cells ($r = 0.7832$, $P < 0.0001$; and $r = 0.9091$, $P < 0.0001$, respectively). Bars: (A) 0.5 μm ; (B and C) 1 μm ; (E) 5 μm .



are rather prominent (Fiala et al., 1998). PSD-95 transfection resulted in a significant increase in the number of MISs (mean number: EGFP control, $2.0 \pm 1.3\%$; nontransfected, $1.8 \pm 1.1\%$; PSD-95, $29.1 \pm 2.9\%$; $P < 0.01$; Fig. 3 C) and in their complexity. On some dendritic segments, their occurrence increased markedly, as illustrated in Fig. 3 E in which 16 out of 28 spines exhibited synaptic contacts with multiple presynaptic terminals. The increased complexity of these structures is indicated by the number of presynaptic terminals making contact with a single spine (Fig. 3 E). This number varied between two and seven in

PSD-95-transfected cells, whereas the maximum observed under control conditions was only two (see Fig. S2 for a distribution of the number of contacts). Furthermore, in the case of MISs, the individual PSDs could show a complex organization with perforated or segmented PSDs in the synaptic contacts made by several axons on the same spine (Videos 1 and 2). A final characteristic of MISs is their unusually large size ($0.29 \pm 0.028 \mu\text{m}^3$ compared with $0.064 \pm 0.011 \mu\text{m}^3$ in EGFP-transfected cells) and the fact that they exhibit large PSD areas both at individual contacts ($0.164 \pm 0.012 \mu\text{m}^2$ compared with $0.033 \pm 0.004 \mu\text{m}^2$ in

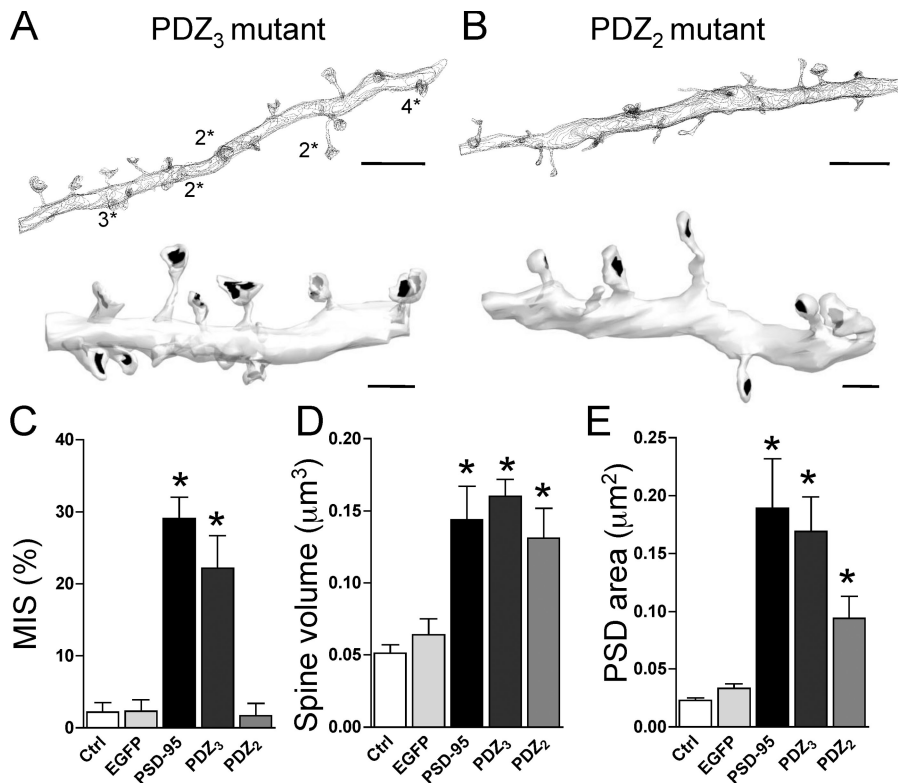


Figure 4. Deletion of the PDZ₂ but not the PDZ₃ domain of PSD-95 prevents MIS formation. (A, top) Contour representation of a dendritic segment reconstructed from a PDZ₃ mutant PSD-95-overexpressing cell illustrating the preservation of numerous MISs (numbers refer to presynaptic terminals [*] making synaptic contacts on the spine). (bottom) Three-dimensionally reconstructed segment expressing PDZ₃ mutant PSD-95 illustrating large, complex spines. (B, top) Same as in A (top) but for a PDZ₂ mutant PSD-95. Note the absence of MISs. (bottom) Same as in A (bottom) but for a cell expressing PDZ₂ mutant PSD-95. MISs are absent, but large spines are still present. (C) Quantitative analysis of the proportion of MISs observed under control conditions (ctrl; $n = 8$ cells; 145 spines) and in cells transfected with EGFP ($n = 4$ cells; 164 spines), PSD-95 ($n = 7$ cells; 234 spines), PDZ₃ mutant PSD-95 ($n = 3$ cells; 86 spines), and PDZ₂ mutant PSD-95 ($n = 3$ cells; 56 spines; *, $P < 0.05$ vs. control and PDZ₂). (D) Same as in C but for the spine volume. Expression of PDZ mutants of PSD-95 does not prevent PSD-95-induced spine enlargement (*, $P < 0.05$ vs. control). (E) Same as in C but for the total PSD area. Expression of PDZ mutants of PSD-95 does not reduce or only partially reduces the increase in PSD area (*, $P < 0.05$ vs. control). Data are mean \pm SEM (error bars). Bars: (A and B, top) 5 μm ; (A and B, bottom) 1 μm .

EGFP-transfected cells; $n = 190$ and 175 PSDs, respectively; $P < 0.01$) and on the entire spine (sum of all PSDs on a given spine, $0.466 \pm 0.047 \mu\text{m}^2$; $n = 68$ MISs; Fig. 3 F).

Role of PSD-95 in MIS formation

To understand how PSD-95 overexpression could induce multiple axons to form synapses on a given spine, we examined which region of the protein could be involved in these effects. Numerous interactions of PSD-95 occur through its PDZ domains that typically bind PDZ domains or specific carboxy-terminal sequences in target proteins. We started by generating PSD-95 mutants with deletions in the PDZ₂ and PDZ₃ regions. PDZ₂ binds synaptic GTPase-activating protein, an adhesion molecule implicated in the regulation of synapse formation (Kim et al., 1998; Vazquez et al., 2004), and neuronal NOS (nNOS), the source of a possible trans-synaptic messenger (Tochio et al., 2000; Sunico et al., 2005), whereas the PDZ₃ domain is involved in interactions with neuroligin, another adhesion molecule implicated in synapse formation mechanisms (Prange et al., 2004; Gerrow et al., 2006). These mutant PSD-95-EGFP constructs were then transfected in pyramidal neurons, and the cells were processed for EM analyses.

Fig. 4 (A and B) shows three-dimensionally reconstructed dendritic segments from cells transfected with each of those constructs. Interestingly, expression of PDZ₃ mutant PSD-95 in neurons still resulted in numerous MISs (Fig. 4, A and C). Their proportion did not change, nor did the mean spine volume or PSD area of three-dimensionally reconstructed spines as compared with PSD-95-transfected neurons (MISs, $22.1 \pm 4.5\%$ vs. $29.1 \pm 2.9\%$; spine volume, $0.168 \pm 0.012 \mu\text{m}^3$ vs. $0.144 \pm 0.023 \mu\text{m}^3$; PSD area, $0.169 \pm 0.03 \mu\text{m}^2$ vs. $0.189 \pm 0.043 \mu\text{m}^2$; $n = 3$

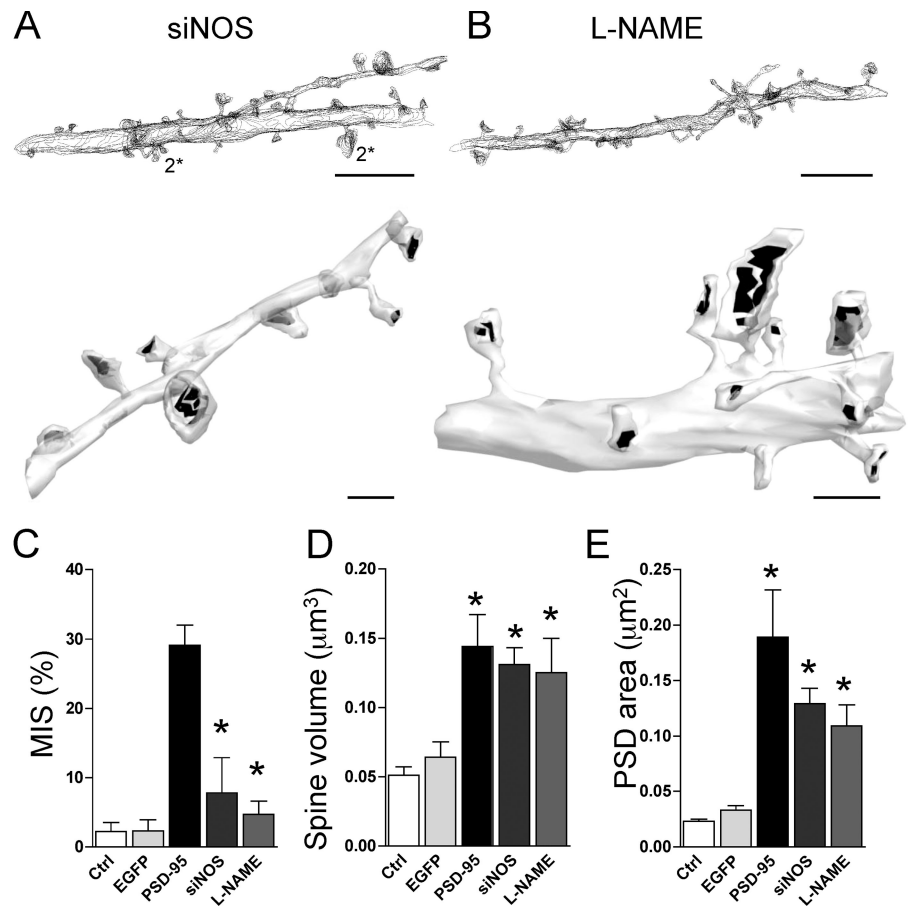
and 7 cells for PDZ₃ mutant and PSD-95-transfected cells, respectively; Fig. 4, C–E). In contrast, the number of MISs markedly decreased in cells expressing the PDZ₂ mutant PSD-95 (PDZ₂ mutant, $1.7 \pm 1.7\%$ vs. PSD-95, $29.1 \pm 2.9\%$; $n = 3$ and 7 cells, respectively; $P < 0.01$; Fig. 4, B and C), reaching values similar to those found in control cells (neighboring, nontransfected neurons, $2.0 \pm 1.3\%$; $n = 8$ cells). The mean spine volume, however, remained significantly enlarged compared with control cells ($0.131 \pm 0.021 \mu\text{m}^3$; $P < 0.05$) as well as the mean PSD area ($0.094 \pm 0.019 \mu\text{m}^2$; $P < 0.05$; Fig. 4, D and E). Thus, expression of a PDZ₂ mutant PSD-95 resulted in the enlargement of spines with increased PSD areas but specifically prevented formation of multiinnervated structures.

Role of NOS in MIS formation

As the PDZ₂ domain of PSD-95 is involved in interactions with different partners and because we previously found that NO could affect axonal varicosity remodeling (Nikonenko et al., 2003), we tested the role of nNOS and NO in the formation of MISs. For this, we performed two groups of experiments to examine whether suppression of NOS activity in cells overexpressing PSD-95 prevented the formation of MISs. First, we used an NOS siRNA, which markedly inhibited nNOS expression in fibroblasts (Fig. S3, available at <http://www.jcb.org/cgi/content/full/jcb.200805132/DC1>) and also interfered with NOS expression at synapses (see Fig. 6). Second, we transfected pyramidal neurons with PSD-95-EGFP and treated the slice cultures for 2 d after transfection with 200 μM of the NOS inhibitor L-N^G-nitroarginine methyl ester (L-NAME) in the culture medium. This treatment did not induce any toxicity, as indicated by propidium iodide staining (unpublished data). Slice cultures

Figure 5. Knockdown and pharmacological blockade of nNOS prevents MIS formation.

(A) Contour representation (top) and 3D reconstruction (bottom) of a dendritic segment obtained from a cell cotransfected with PSD-95 and an siRNA against nNOS (siNOS). Note the small number of MISs (top; numbers refer to presynaptic terminals [*] making synaptic contacts on the spine) and the persistence of larger spines (top and bottom). (B) Same as in A but for a PSD-95-transfected cell treated for 2 d with 200 μ M of the NOS inhibitor L-NAME. L-NAME prevented MIS formation (top) but not the PSD-95-induced spine and PSD enlargement (bottom). (C) Quantitative analysis illustrating the proportion of MISs detected under control conditions (ctrl; $n = 8$ cells; 145 spines) and in cells transfected with EGFP ($n = 4$ cells; 164 spines), PSD-95 ($n = 7$ cells; 234 spines), PSD-95 and siNOS ($n = 5$ cells; 127 spines), and PSD-95 treated with L-NAME ($n = 4$ cells; 128 spines). Both siNOS transfection and L-NAME treatment significantly prevented MIS formation (*, $P < 0.05$ vs. PSD-95). (D) Same as in C but for the spine volume. siNOS transfection and L-NAME treatment did not prevent PSD-95-induced spine enlargement (*, $P < 0.05$ vs. control). (E) Same as in C but for the total PSD area. siNOS transfection and L-NAME treatment only partially reduced the PSD enlargement associated with PSD-95 overexpression (*, $P < 0.05$ vs. control). Data are mean \pm SEM (error bars). Bars: (A and B, top) 5 μ m; (A and B, bottom) 1 μ m.



were then processed for EM analyses. As illustrated in Fig. 5, both down-regulation of NOS by the siRNA approach and treatment of slice cultures with the NOS inhibitor prevented the formation of MISs. The decrease was partial but significant with nNOS siRNA transfection ($7.8 \pm 5.1\%$; $n = 5$ cells), whereas the blockade of MIS formation was complete with L-NAME treatment of PSD-95-transfected neurons ($4.4 \pm 1.9\%$, $n = 4$ cells vs. $2.0 \pm 1.3\%$, $n = 8$ cells for control; $29.1 \pm 2.9\%$, $n = 7$ cells for PSD-95; Fig. 5 C). Interestingly, the increase in spine volume and PSD area associated with PSD-95 overexpression was not blocked by these manipulations (spine volume, $0.131 \pm 0.012 \mu\text{m}^3$ and $0.125 \pm 0.025 \mu\text{m}^3$; PSD area, $0.129 \pm 0.014 \mu\text{m}^2$ and $0.118 \pm 0.016 \mu\text{m}^2$ for siNOS [silencing RNA for NOS] and L-NAME, respectively; Fig. 5, D and E).

Interaction between PSD-95 and nNOS expression

If PSD-95 regulates MIS formation through its interaction with nNOS, one would expect that modifications of PSD-95 expression should affect nNOS expression. To investigate this possibility and the level of expression of these two proteins, we compared by immunohistochemistry the size of PSD-95- and nNOS-immunostained puncta and their colocalization under four experimental conditions: control situation, PSD-95 overexpression, expression of the PDZ₂ mutant of PSD-95, and, finally, overexpression of PSD-95 together with nNOS siRNA. Fig. 6 illustrates PSD-95- and nNOS-immunostained PSD

spots as visualized by confocal microscopy in the CA1 stratum radiatum. Under control conditions, small nNOS puncta (Fig. 6 A, red), which are usually smaller than PSD-95-labeled puncta (Fig. 6 A, blue), are seen everywhere in the dendritic region. They often colocalize with PSD-95 staining (Fig. 6 A, right), confirming the presence of nNOS at excitatory synapses. However, not all PSD-95-stained puncta express a detectable amount of nNOS, and there are nNOS puncta that do not colocalize with PSDs. In areas containing cell dendrites of PSD-95-EGFP-transfected neurons (Fig. 6 B, green PSD spots), PSD-95 immunostaining (Fig. 6 B, blue PSD spots) perfectly reveals the same PSD spots as EGFP together with a few other spots on neighboring cells. Comparisons of the size of PSD-95-immunostained puncta on PSD-95-transfected and nontransfected cells shows a 5.4 \times increase in the size of PSD spots, a result that reflects the increased level of expression of PSD-95 in transfected cells ($n = 4$ PSD-95-transfected cells; 95 and 105 puncta analyzed; $P < 0.01$; Fig. S4, available at <http://www.jcb.org/cgi/content/full/jcb.200805132/DC1>). Note that in all other conditions of transfection analyzed in this study (PDZ₂, PDZ₃, and PSD-95 + siNOS), the increase in size of PSD-95-immunostained puncta is comparable, suggesting a similar level of expression of the different constructs used (Fig. S4). Most importantly, however, immunostaining reveals that the size of nNOS puncta in PSD-95-transfected cells is also markedly larger (factor of 6.4; $n = 4$ cells; $P < 0.05$; Fig. 6 E), indicating that PSD-95 overexpression is indeed associated with a concomitant increase

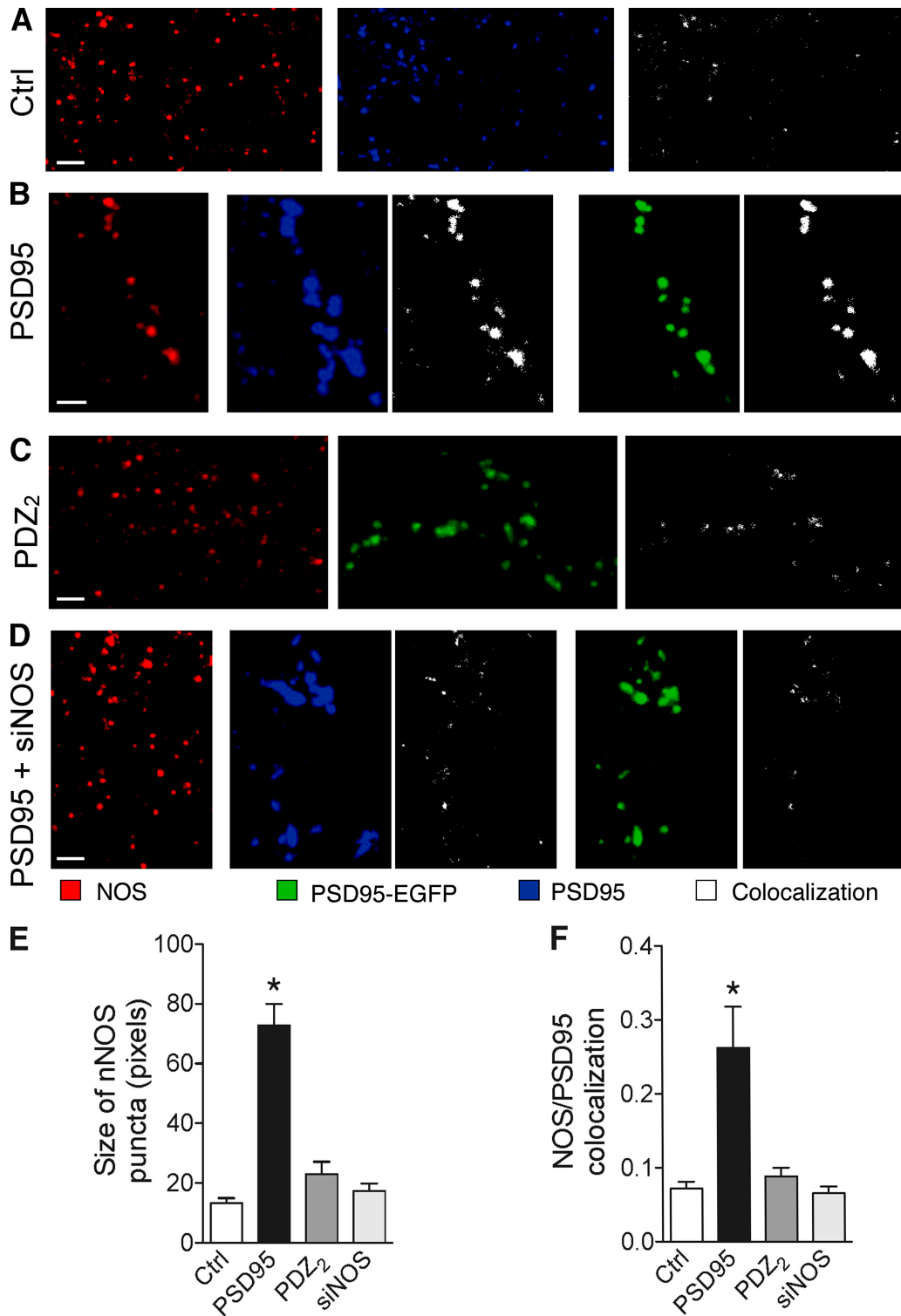
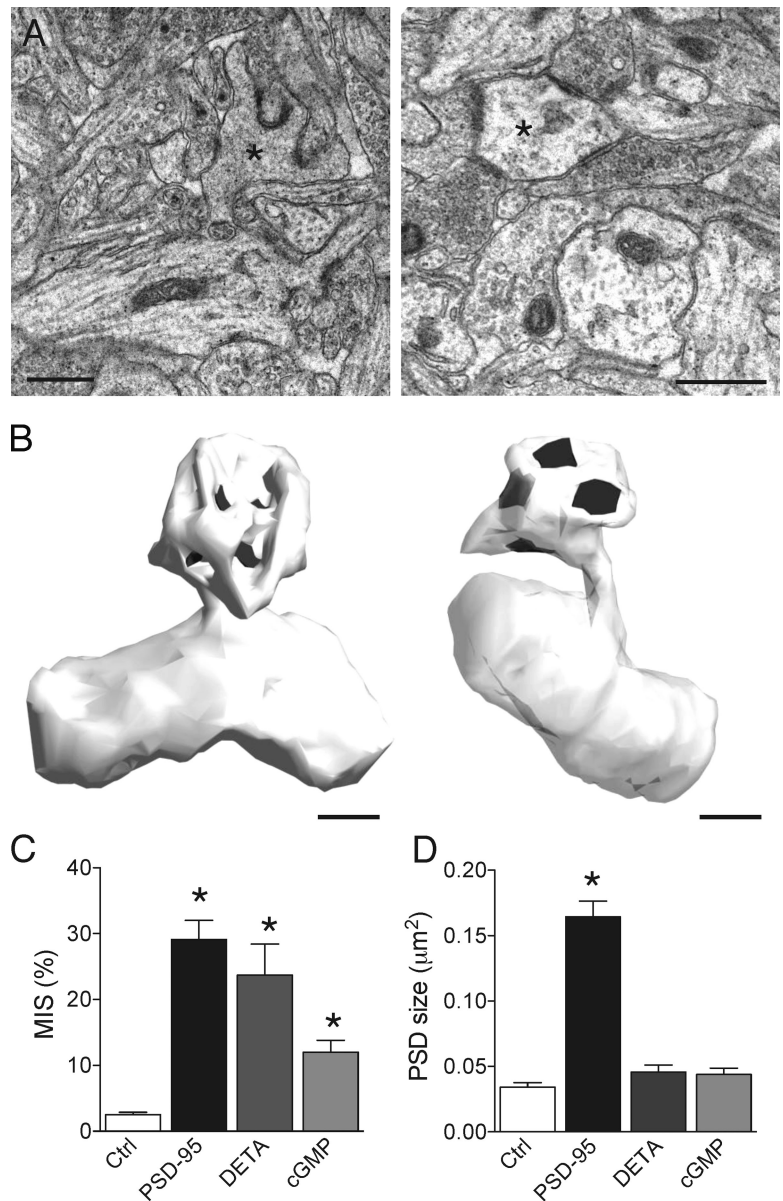


Figure 6. PSD-95 overexpression correlates with increased nNOS expression at synapses. (A) Immunostaining against nNOS (red) and PSD-95 (blue) and their colocalization (white) obtained in the same field of stratum radiatum of a control hippocampal slice culture. Note the existence of PSD-95 puncta devoid of nNOS staining as well as nNOS puncta negative for PSD-95. (B) Same as in A but in a field containing a dendritic segment from a PSD-95-EGFP-transfected neuron (green). Colocalization between nNOS and PSD-95 immunostainings or nNOS and PSD-95-EGFP fluorescence are shown in white. Note the enlargement of the PSD-95 puncta and the presence of large nNOS-positive spots associated with the PSD-95 puncta. (C) Same as in A but in a field containing a dendritic segment from a PDZ₂ mutant PSD-95-EGFP-transfected neuron. Note the reduced size of nNOS puncta associated with PSD-95-EGFP staining. (D) Same as in A but in a field containing a dendritic segment from a cell cotransfected with PSD-95-EGFP and nNOS siRNA. Note again the reduced nNOS staining associated with PSD-95 puncta. (E) Analysis of the size of nNOS puncta measured as the number of stained pixels under the different conditions analyzed. Data are mean \pm SEM (error bars) of the analysis of four different slice cultures (75–105 puncta analyzed per condition; *, $P < 0.05$; Mann-Whitney test). (F) Colocalization between nNOS and PSD-95 immunostaining (or PSD-95-EGFP fluorescence for the PDZ₂ condition) measured in 9–21 different fields (30 \times 30 μ m) obtained from four different slice cultures per condition (*, $P < 0.05$; Mann-Whitney test). Data are mean \pm SEM (error bars). Bars, 2 μ m.

Figure 7. Increased formation of MISs by the NO donor DETA NONOate and the cell-permeable cGMP analogue 8-Br-cGMP. (A) EM sections illustrating the presence of MISs (asterisks) in slice cultures treated for 2 d with 150 μ M DETA NONOate (left) or 5 mM 8-Br-cGMP (right). (B) 3D reconstruction of the two MISs illustrated in A, the left and right spines making synaptic contacts with five and four different axons, respectively. (C) Proportion of MISs observed in randomly selected volume samples of CA1 stratum radiatum in the control situation (ctrl; three slices and 615 spines analyzed), in DETA NONOate-treated cultures (DETA; three slices and 583 spines analyzed), and in 8-Br-cGMP-treated slices (cGMP; three slices and 963 spines analyzed) compared with the analysis of 234 spines in PSD-95-transfected cells (seven slices). Data are mean \pm SEM (error bars; *, $P < 0.01$). (D) Size of individual PSDs on spines from control slices and on MISs of PSD-95-transfected cells and of DETA NONOate- or of 8-Br-cGMP-treated cultures. Data are mean \pm SEM (error bars) of 114–269 reconstructed PSDs (*, $P < 0.01$). Bars, 0.5 μ m.



of nNOS expression at the same synapse. As a result, the level of colocalization between PSD-95 and nNOS immunostaining also markedly increased ($n = 4$; $P < 0.05$; Fig. 6 F). In contrast, in cells transfected with the PDZ₂ mutant of PSD-95 or with PSD-95 + siNOS, the enlargement of PSD-95 puncta is not associated with a similar change of nNOS puncta; they remain small (Fig. 6, C–E), and the level of colocalization of nNOS and PSD-95 immunostaining is essentially unchanged (Fig. 6 F), confirming the role of PSD-95 in regulating the level of nNOS expression at excitatory synapses.

Role of NO in MIS formation

If NO is indeed responsible for MIS formation, their frequency should increase by exogenous application of NO or by activating signaling cascades associated with NO such as cyclic guanosine monophosphate (cGMP) formation. To test this, we incubated slice cultures for 2 d with 150 μ M of the NO donor diethylenetriamine (DETA) NONOate or with the cell-permeable cGMP

analogue 8-Br-cGMP (8-bromo-cGMP sodium salt). As illustrated in the EM pictures and 3D reconstructions of Fig. 7 A, these two conditions resulted in MIS formation in the entire tissue. Using serial sections and 3D reconstructions, we analyzed 2,161 spines in randomly chosen volumes in stratum radiatum taken from nine different slice cultures and determined the proportion of MISs. This proportion increased from $2.5 \pm 0.3\%$ under control condition to $23.7 \pm 4.7\%$ after DETA NONOate treatment and, thus, is very close to the values obtained in PSD-95-transfected cells ($n = 3$ cultures for each condition; 615 and 583 spines analyzed; $P < 0.01$; Fig. 7 C). Furthermore, DETA NONOate treatment increased MISs not only on all cells of treated cultures but also on cells overexpressing the PDZ₂ mutant of PSD-95 ($32.9 \pm 8.6\%$ of MISs; $n = 4$; $P < 0.05$; Table S1), indicating that the effect of NO is indeed downstream of PSD-95. Similarly, the application of 5 mM 8-Br-cGMP increased the proportion of MISs in the entire tissue to $12.0 \pm 1.8\%$ ($n = 3$ cultures; 963 spines analyzed; $P < 0.01$). Conversely, the

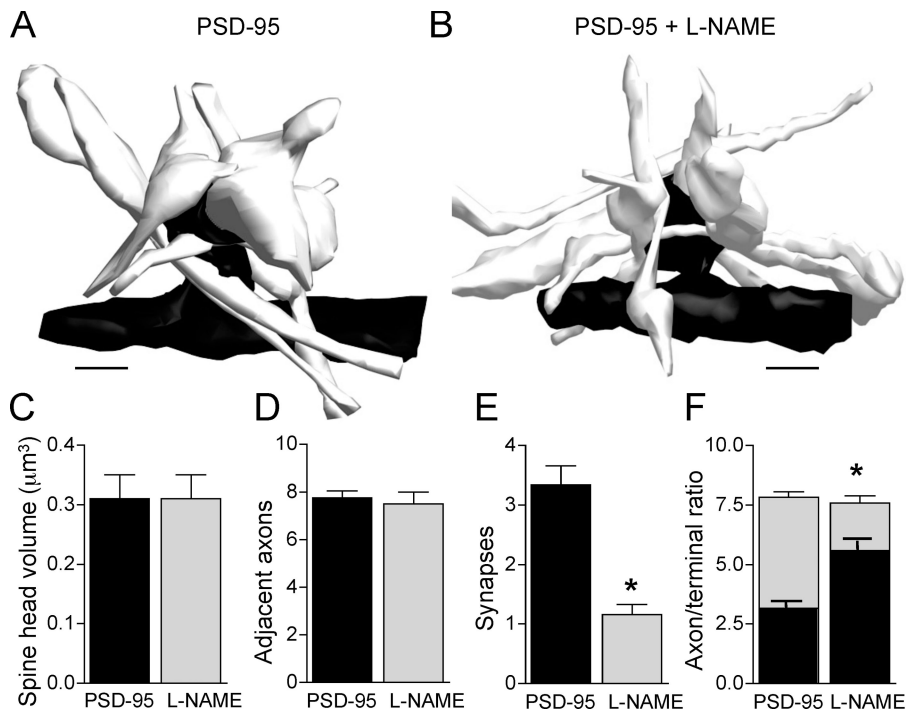


Figure 8. NO promotes axonal varicosities differentiation and regulates spine and synapse formation under control conditions. (A) 3D reconstruction of an MIS and adjacent axons observed upon PSD-95 transfection. Seven axons were present in the vicinity, four of which made a synaptic contact. (B) 3D reconstruction of an enlarged spine observed upon PSD-95 transfection but with L-NAME treatment illustrating seven axons also present in the vicinity, of which only one made a synaptic contact. (C) 3D analysis of the environment of 12 MISs observed upon PSD-95 transfection and 12 large spines observed upon L-NAME treatment of PSD-95-transfected cells. Selection was based on similar spine head volumes. (D) The number of axons directly adjacent to the enlarged spines was similar in both conditions (7.8 ± 0.3 vs. 7.6 ± 0.5 axons; $n = 12$ spines). (E) The number of synaptic contacts made by adjacent axons is decreased by L-NAME treatment of PSD-95-transfected cells (*, $P < 0.05$). (F) The ratio of axonal shafts (black bars) versus axonal varicosities (gray bars; defined by the presence of vesicles + enlargement) is modified by L-NAME treatment ($n = 12$ spines; *, $P < 0.05$). Data are mean \pm SEM (error bars). Bars, $1 \mu\text{m}$.

blockade of cGMP by $25 \mu\text{M}$ of the inhibitor ODQ (*1H*-[1,2,4]oxadiazole[4,3- α]quinoxalin-1-one) prevented formation of MISs on PSD-95-transfected neurons ($7.2 \pm 0.5\%$; $n = 3$; Table S1). Interestingly, although both the NO donor and cGMP analogue promoted MIS formation, the PSDs expressed on these MISs did not differ in size from those measured under control conditions (Fig. 7 D). Thus, NO production is sufficient for the generation of MISs and does not require overexpression of PSD-95.

Mechanism of NO-mediated MIS formation

We then investigated whether NO promoted multiple contact formation by attracting axons toward PSD-95-overexpressing spines or whether it rather favored axonal varicosity differentiation and synaptic contact formation with axons already present in the vicinity of the spine. For this, we analyzed the number of axons in contact with 12 reconstructed MISs from PSD-95-transfected cells and 12 spines from cells overexpressing PSD-95 that were treated with L-NAME. Reconstructed spines were selected so as to exhibit exactly the same size (Fig. 8, A–C). However, the mean number of synapses established with each spine was much higher in PSD-95-transfected cells (3.33 ± 0.32 vs. 1.17 ± 0.17 in PSD-95- and L-NAME-treated cells, respectively; $P < 0.05$; Fig. 8 E). Interestingly, the number of axons found in close proximity to the spine membrane was actually similar (7.8 ± 0.3 for PSD-95 vs. 7.6 ± 0.5 for L-NAME; Fig. 8 D). However, these axons mainly exhibited features of differentiated terminals in the case of PSD-95-transfected cells (enlargement and presence of vesicles, including docked vesicles; 4.7 ± 0.2 axonal varicosities and 3.1 ± 0.2 axonal shafts), whereas they mainly corresponded to axonal shafts in the case of L-NAME treatment (2 ± 0.3 varicosities and 5.6 ± 0.4 axonal shafts; $P < 0.05$; Fig. 8 F). Therefore, the main effect of NO was to promote presynaptic terminal differentiation and formation of a synaptic contact by the axons already present in the direct vicinity of the spine.

Physiological role of NO in spine synapse formation

We then asked whether NO also contributed to synapse formation under control conditions. For this, we examined the morphology and density of spines in slice cultures treated for 2 d with the NOS inhibitor L-NAME. This condition clearly affected the mechanisms of spine and synapse formation as both the density of spines and of synapses considerably decreased upon L-NAME treatment (0.65 ± 0.11 spines/ μm vs. 1.08 ± 0.12 spines/ μm and 0.72 ± 0.12 synapses/ μm vs. 1.2 ± 0.12 synapses/ μm ; $n = 8$ cells; $P < 0.05$; Fig. 9, A and B; and Table S1). However, the morphology of remaining spines was not affected, as both the spine volume and PSD area were only slightly different from the values obtained in control tissue ($0.078 \pm 0.016 \mu\text{m}^3$ and $0.042 \pm 0.008 \mu\text{m}^2$), and the number of MISs was also very low ($1.7 \pm 1.7\%$). Thus, synapse formation under control conditions also appears to require NO signaling to be effective.

Discussion

This study examined the morphological properties of excitatory synapses upon overexpression of PSD-95 and reveals important new functions of this protein in regulating spine synapse formation and plasticity. The expression of PSD-95 resulted in changes in spine shape, a marked increase of the spine volume, and an enlargement of the PSD, resulting in the formation of synapses with complex and perforated or segmented PSDs. The effect is very significant because, on average, the PSD area increased by a factor of six to eight, and the spine volume increased about threefold, emphasizing the close relationship existing between spine volume and PSD size (Harris and Stevens, 1989; Harris et al., 1992). These results are consistent with the notion that PSD-95, as a major scaffold protein, shapes the PSD and regulates the

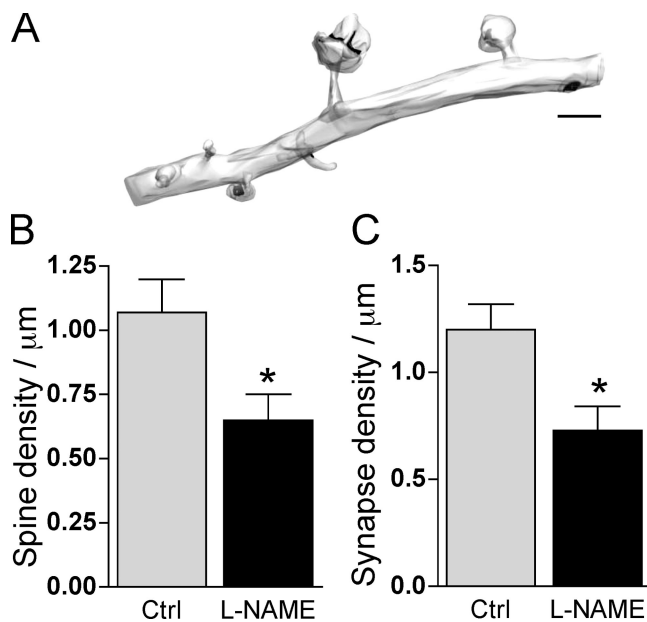


Figure 9. NO regulates spine and synapse formation under control conditions. (A) 3D reconstruction of a dendritic segment from a control pyramidal neuron treated for 2 d with 200 μ M L-NAME. Note the decrease in spine density. (B) Quantitative analysis of the spine density measured in control (ctrl; $n = 8$ cells; total length = 134 μ m; 145 spines) and L-NAME-treated slice cultures ($n = 8$ cells; total length = 99 μ m; 59 spines; *, $P < 0.05$). (C) Same as in B but for the synapse density measured by analyzing all PSDs per micrometer of length on dendritic segments of control and L-NAME-treated slice cultures ($n = 8$ cells; *, $P < 0.05$). Data are mean \pm SEM (error bars). Bar, 1 μ m.

expression of several proteins or receptors that are important for synaptic function and plasticity (Stein et al., 2003; Xu et al., 2008), including NOS (Chen et al., 2000; Ishii et al., 2006). This probably accounts for the general increase in synaptic efficacy and AMPA receptor-mediated currents reported at individual synapses in PSD-95-transfected cells (Stein et al., 2003; Ehrlich and Malinow, 2004). It is also interesting that the changes associated with PSD-95 overexpression share many similarities, both at the functional and morphological level, with those reported after LTP induction. At the functional level, PSD-95 overexpression mimics and occludes LTP (Stein et al., 2003; Ehrlich and Malinow, 2004), whereas at the morphological level, the two situations seem to involve an enlargement of the spine and the formation of spines with complex, perforated PSDs (Geinisman, 1993; Buchs and Muller, 1996; Matsuzaki et al., 2004). One possibility with regard to these changes in spine volume and efficiency is that they promote spine stability (Kasai et al., 2003).

The most intriguing finding of this study, however, is the observation that overexpression of PSD-95 results in the formation of MISs. Although dendritic spines connected by two distinct presynaptic terminals can occasionally be found in the hippocampus, their number is usually low, in the range of a few percentages (Fiala et al., 1998; Nikonenko et al., 2003). However, MISs are regulated under various conditions involving enhanced synaptogenesis such as the blockade of synaptic transmission (Pettrak et al., 2005) or induction of plasticity (Nikonenko et al., 2003). There is also one study suggesting the existence of MISs in a hibernating mammal (Popov et al., 2005). In this study, we

found that overexpression of PSD-95 increased their occurrence by a factor of 10 as well as their complexity because MISs contacted by three to seven different axon terminals were frequently observed. It is interesting that these conditions of enhanced spine innervation and synaptic efficacy were actually associated with a reduction of spine density. The mechanisms remain unclear but could involve a kind of homeostatic process through which activity may regulate the number of synapses.

The importance of these findings resides in the new understanding of the role of PSD-95 and of its interaction with nNOS for mechanisms of synaptogenesis and their regulation of presynaptic differentiation and contact formation. Our results demonstrate that PSD-95 controls synapse formation through its regulation of nNOS expression at the synapse, the release of NO, and most likely the activation of cGMP signaling in presynaptic axons. This conclusion is supported by several observations: (a) PSD-95 overexpression is associated with an increased expression of nNOS in PSDs and the formation of MISs; (b) deletion of the PDZ₂ domain of PSD-95 specifically prevented the increased expression of nNOS and the formation of MISs; (c) overexpression of PSD-95 together with siRNA down-regulation of nNOS also markedly reduced nNOS expression at the synapse and prevented formation of MISs; (d) the pharmacological blockade of nNOS prevented MIS formation; and, conversely, (e) the exogenous application of the NO donor DETA NONOate or enhancement of cGMP signaling, a classical downstream target of NO, reproduced MIS formation in the entire slice culture and without alterations of PSD size. Also, DETA NONOate treatment was able to rescue the absence of MISs in PDZ₂-transfected cells, and, finally, the pharmacological blockade of nNOS interfered with spine and synapse development under control conditions. Thus, PSD-95 and nNOS are key regulators of the mechanisms of synapse formation.

This conclusion is consistent with and could account for the defects in synapse development reported upon suppression of PSD-95 (Ehrlich et al., 2007). This is also in line with the variations in spine density found in various brain areas in PSD-95 knockout mice (Vickers et al., 2006), although some compensatory mechanisms could probably be involved. Most importantly, however, these results may help to understand the function of PSD-95 in the stabilization of new synapses. During development, spine turnover in cortical structures is rather high (Holtmaat et al., 2005; Zuo et al., 2005; De Roo et al., 2008), and recent evidence indicates that newly formed spines do initially grow without a PSD and possibly without a presynaptic partner (Knott et al., 2006; Arellano et al., 2007; De Roo et al., 2008). PSDs, and particularly PSD-95, start to be expressed after a few hours, a step that is critical for the stabilization of the newly formed spine (Marrs et al., 2001; Prange and Murphy, 2001; De Roo et al., 2008). Our current results suggest a scenario in which PSD-95 expression at a new protrusion, through association with nNOS and NO production, would stimulate the differentiation of a close-by axon into a presynaptic varicosity and the establishment of a morphologically mature synapse. NO release would therefore represent a signal informing axons in the vicinity of the existence of a potential postsynaptic partner, and absence of NO or failure of axons to respond could then result in elimination of the protrusion.

Upon overexpression of PSD-95, this mechanism is overemphasized, and more axons located around the spine become stimulated by NO, start to differentiate into varicosities, and then form MISs, an effect that could be mediated by activation of cGMP signaling in presynaptic structures. Alternatively, the excess of NO release could represent a local neurotoxic situation to which axons respond by increasing synaptogenesis. Although difficult to exclude, this possibility seems unlikely because MISs are formed exclusively with PSD-95-overexpressing spines and not with other spines in the area, indicating specificity. Furthermore, the role of PSD-95 and NO uncovered in this study is likely to be physiologically relevant for different reasons. First, it certainly operates under control conditions for the formation of synapses involving a single presynaptic partner because, as shown in this study, the acute blockade of nNOS resulted in a marked reduction in the density of dendritic spines and of synapse formation. Second, these mechanisms can also account for the formation of MISs both in control brain tissue and under conditions in which MISs are increased, such as after the blockade of synaptic transmission (Petra et al., 2005) or induction of synaptic plasticity (Nikonenko et al., 2003). A role for NO in these mechanisms would actually be in line with previous work showing that the application of an NO donor to hippocampal slice cultures results in an increased dynamic and growth of presynaptic varicosities (Nikonenko et al., 2003). Third, this mechanism could also account for the observation that newly formed spines in adult tissue or on newly generated neurons very often target existing terminals (Knott et al., 2006; Toni et al., 2007), providing a means through which newly formed dendritic protrusions can enter into competition with preexisting synaptic contacts. The role of PSD-95 in regulating these mechanisms might therefore be instrumental for the stabilization and pruning of synaptic networks and emphasizes the critical role played by the postsynaptic structure in driving the selection of the presynaptic partner. Finally, these mechanisms might also be implicated in some neuropathological aspects because multi-innervated giant spines have been reported along Purkinje cells during malnutrition or in the cortical tissue surrounding tumors (Chen and Hillman, 1980; Fiala et al., 2002). Excessive expression of PSD-95 or nNOS under these conditions could account for these abnormalities. In conclusion, the molecular regulation between PSD-95 and nNOS uncovered in this study provides a new mechanism through which postsynaptic structures can promote synapse formation.

Materials and methods

Slice cultures, constructs, and siRNAs

Organotypic hippocampal slice cultures were prepared from 7-d-old rat pups as previously described (Stoppini et al., 1991), and all experiments were performed with slice cultures maintained 11–15 d *in vitro* (DIV).

The PSD-95–EGFP fusion construct prepared in the GW1 mammalian expression vector was a gift from D.S. Bredt (University of California, San Francisco, San Francisco, CA). The vectors PSD-95–EGFP-PDZ₂ and PSD-95–EGFP-PDZ₃ were produced using the same strategy. The plasmids produced after ligation and transformation have been verified by enzyme restriction, sequencing, and Western blot analyses through fibroblast cell line transfection. siRNAs were obtained from QIAGEN (HiPerformance GenomeWide duplexes). The target sequence for rat nNOS was 5'-CAGGAGATGCTCAACTATAGA-3'. As a control, we used the

AllStar Negative Control siRNA, which has no sequence homology in the mammalian genome.

Transfections and immunoblots

Mouse NIH 3T3 fibroblasts, which do not express endogenous nNOS, were transfected with rat nNOS by Lipofectamine 2000 (Invitrogen) or cotransfected with nNOS and either the siRNA against nNOS or the non-silencing siRNA. 48 h after transfection, the fibroblasts were harvested, and total protein was extracted. 30 µg of proteins was separated by SDS-PAGE (NuPAGE; Invitrogen), transferred to nitrocellulose membrane, and incubated with 1:1,000 anti-nNOS rabbit polyclonal antibody (Millipore) and 1:10,000 anti-β-actin mouse antibody (Sigma-Aldrich) followed by anti-mouse and anti-rabbit IgG HRP conjugates (Bio-Rad Laboratories) before detection using ECL (GE Healthcare).

Organotypic hippocampal cultures were transfected or cotransfected at 11 DIV with the different constructs using the hand-held Gene Gun biolistic technique (DNA-coated gold microcarriers; 1.6 µm; Bio-Rad Laboratories) according to the instructions of the manufacturer. Usually, one out of four transfected slice cultures (with 1–10 transfected pyramidal cells per slice) showed efficient transfection of pyramidal cells. The transfection of other cell types could also occur, but less reliably. Only one transfected CA1 pyramidal cell per slice was analyzed in this study. Transfected cells were used for morphological experiments 2 d after transfection.

Immunohistochemistry

To reveal PSD-95 and nNOS molecules, we applied a proteolytic treatment known to unmask hidden antigenic epitopes (modified from Burette et al., 2002). Immunostaining was performed using the following antibodies: 1:8,000 primary anti-nNOS rabbit polyclonal antibody (Millipore) applied overnight at 4°C followed by 1:1,000 secondary anti-rabbit antibodies (Alexa Fluor 555; Invitrogen) applied for 2 h at room temperature and 1:20,000 primary anti-PSD-95 mouse monoclonal antibody (Thermo Fisher Scientific) applied overnight at 4°C followed by 1:1,000 secondary anti-mouse antibodies (Alexa Fluor 647; Invitrogen) applied for 2 h at room temperature. The images were taken with a confocal microscope (LSM 510; Ar laser 458/488/514 nm, 25 mW; HeNe 543 nm, 1 mW; HeNe 633 nm, 5 mW; Carl Zeiss, Inc.) using a Plan-Apochromat 63× NA 1.4 oil objective. Colocalization was analyzed using ImageJ software (National Institutes of Health) and the colocalization plug-in with the same default threshold parameters for all images analyzed. Colocalization was then quantified for fields of the same size (512 × 512 pixels; 30 × 30 µm) on a single confocal plane by calculating the number of pixels positive for two different stains. We verified that a shift of 15 pixels in the xy plane reduced the level of colocalization by a factor of three and prevented the increase detected in PSD-95-expressing cells.

Electron microscopy

After the imaging of transfected cells in a confocal spinning-disk microscope (Visitron Systems) with MetaMorph software (Visitron Systems), the slice cultures were fixed with 2% paraformaldehyde and 0.2% glutaraldehyde in 0.1 M phosphate buffer, pH 7.4, cryoprotected, freeze thawed in liquid nitrogen, and incubated overnight in 1:500 primary rabbit anti-GFP antibody (Millipore) at 4°C and then in 1:200 biotinylated secondary goat anti-rabbit antibody (Jackson ImmunoResearch Laboratories) and avidin biotin peroxidase complex (Vector Laboratories) followed by 3,3'-diaminobenzidine tetrachloride and 0.015% hydrogen peroxide. After embedding in EPON resin (Fluka), the cultures were trimmed for cutting around labeled cells of interest, and 60-nm serial ultrathin sections were cut. Images of labeled dendrites from the middle portion of CA1 stratum radiatum were taken at a magnification of 9,700–15,000 using transmission electron microscopes (Philips CM10, Philips CM12, and Tecnai G212; FEI Company) equipped with digital cameras (Mega View III and Morada; Soft Imaging Systems). Synapses were defined by the presence of a PSD facing at least two to three presynaptic vesicles. Complex or perforated PSDs were defined by the presence of a discontinuity on a single section. Terminals were identified by the presence of an enlargement of the axonal shaft containing vesicles and facing at least one PSD.

Digital serial electron micrographs were aligned using Photoshop software (Adobe). 3D reconstructions as well as surface, volume, and length measurements were performed using NeuroLucida software (version 6.02; MicroBrightField, Inc.). 3D illustrations were made using the software Reconstruct developed by J.C. Fiala and K.M. Harris (SynapseWeb: <http://synapses.clm.utexas.edu/tools/index.stm>; Fiala, 2005) followed by color rendering with 3D Studio Max (Discreet Software).

In some experiments, slice cultures (10–11 DIV) were treated for 2 d with either 200 µM of the NOS inhibitor L-NAME, the NO donor DETA

NONOate (20-h half-life in solution, 150 μ M in culture medium; Enzo Biochem, Inc.), or the cell-permeable 8-Br-cGMP (5 mM in culture medium; Enzo Biochem, Inc.). The drugs were added twice at 24-h intervals. Serial thin sections were cut in the middle part of CA1 stratum radiatum, and the proportion of MISs was analyzed in randomly selected volume samples obtained from treated and control tissue, with images taken of at least 40 consecutive sections at a magnification of 9,700–13,500. For each group, three slice cultures from different experiments were used. To analyze spine density in these experiments, 3D reconstructions of spines were performed in the same volume samples on several dendritic segments per culture.

Statistical analysis

Data are shown as mean \pm SEM. Statistical analyses were performed using the Student's *t* test or Mann-Whitney test when indicated.

Online supplemental material

Fig. S1 shows serial sections of an MIS from a PSD-95–transfected cell. Fig. S2 shows the distribution of the number of presynaptic partners in MISs. Fig. S3 shows siNOS activity in fibroblasts. Fig. S4 shows the level of expression of PSD-95 in transfected neurons. Video 1 shows the 3D reconstruction of an MIS contacted by six different axons. Video 2 shows the 3D reconstruction of two MISs on the same dendritic segment. Table S1 shows the summary of morphometric analyses. Online supplemental material is available at <http://www.jcb.org/cgi/content/full/jcb.200805132/DC1>.

We thank Marlis Moosmayer and Lorena Jourdain for excellent technical support, Fred Pillonel for help with Photoshop alignment, and Rudolf Kraftsik for statistical analyses.

This work was supported by the Swiss National Science Foundation (grants 3100-105721 to D. Muller and 310000-108246 to E. Welker) and the European projects Promemoria and Synscalf (grants to D. Muller).

Submitted: 21 May 2008

Accepted: 7 November 2008

References

- Arellano, J.I., A. Espinosa, A. Fairen, R. Yuste, and J. DeFelipe. 2007. Non-synaptic dendritic spines in neocortex. *Neuroscience*. 145:464–469.
- Bats, C., L. Groc, and D. Choquet. 2007. The interaction between Stargazin and PSD-95 regulates AMPA receptor surface trafficking. *Neuron*. 53:719–734.
- Bresler, T., Y. Ramati, P.L. Zamorano, R. Zhai, C.C. Garner, and N.E. Ziv. 2001. The dynamics of SAP90/PSD-95 recruitment to new synaptic junctions. *Mol. Cell. Neurosci.* 18:149–167.
- Buchs, P.A., and D. Muller. 1996. Induction of long-term potentiation is associated with major ultrastructural changes of activated synapses. *Proc. Natl. Acad. Sci. USA*. 93:8040–8045.
- Burette, A., U. Zabel, R.J. Weinberg, H.H. Schmidt, and J.G. Valtschanoff. 2002. Synaptic localization of nitric oxide synthase and soluble guanylyl cyclase in the hippocampus. *J. Neurosci.* 22:8961–8970.
- Chen, L., D.M. Chetkovich, R.S. Petralia, N.T. Sweeney, Y. Kawasaki, R.J. Wenthold, D.S. Bredt, and R.A. Nicoll. 2000. Stargazin regulates synaptic targeting of AMPA receptors by two distinct mechanisms. *Nature*. 408:936–943.
- Chen, S., and D.E. Hillman. 1980. Giant spines and enlarged synapses induced in Purkinje cells by malnutrition. *Brain Res.* 187:487–493.
- Chen, X., L. Vinade, R.D. Leapman, J.D. Petersen, T. Nakagawa, T.M. Phillips, M. Sheng, and T.S. Reese. 2005. Mass of the postsynaptic density and enumeration of three key molecules. *Proc. Natl. Acad. Sci. USA*. 102:11551–11556.
- De Roo, M., P. Klausner, P. Mendez, L. Poglia, and D. Muller. 2008. Activity-dependent PSD formation and stabilization of newly formed spines in hippocampal slice cultures. *Cereb. Cortex*. 18:151–161.
- Ehrlich, I., and R. Malinow. 2004. Postsynaptic density 95 controls AMPA receptor incorporation during long-term potentiation and experience-driven synaptic plasticity. *J. Neurosci.* 24:916–927.
- Ehrlich, I., M. Klein, S. Rumpel, and R. Malinow. 2007. PSD-95 is required for activity-driven synapse stabilization. *Proc. Natl. Acad. Sci. USA*. 104:4176–4181.
- El-Husseini, A.E., E. Schnell, D.M. Chetkovich, R.A. Nicoll, and D.S. Bredt. 2000. PSD-95 involvement in maturation of excitatory synapses. *Science*. 290:1364–1368.
- Fiala, J.C. 2005. Reconstruct: a free editor for serial section microscopy. *J. Microsc.* 218:52–61.
- Fiala, J.C., M. Feinberg, V. Popov, and K.M. Harris. 1998. Synaptogenesis via dendritic filopodia in developing hippocampal area CA1. *J. Neurosci.* 18:8900–8911.
- Fiala, J.C., J. Spacek, and K.M. Harris. 2002. Dendritic spine pathology: cause or consequence of neurological disorders? *Brain Res. Brain Res. Rev.* 39:29–54.
- Funke, L., S. Dakoji, and D.S. Bredt. 2005. Membrane-associated guanylate kinases regulate adhesion and plasticity at cell junctions. *Annu. Rev. Biochem.* 74:219–245.
- Geinisman, Y. 1993. Perforated axospinous synapses with multiple, completely partitioned transmission zones: probable structural intermediates in synaptic plasticity. *Hippocampus*. 3:417–433.
- Gerrow, K., S. Romorini, S.M. Nabi, M.A. Colicos, C. Sala, and A. El-Husseini. 2006. A preformed complex of postsynaptic proteins is involved in excitatory synapse development. *Neuron*. 49:547–562.
- Gray, N.W., R.M. Weimer, I. Bureau, and K. Svoboda. 2006. Rapid redistribution of synaptic PSD-95 in the neocortex in vivo. *PLoS Biol.* 4:e370.
- Harris, K.M., and J.K. Stevens. 1989. Dendritic spines of CA 1 pyramidal cells in the rat hippocampus: serial electron microscopy with reference to their biophysical characteristics. *J. Neurosci.* 9:2982–2997.
- Harris, K.M., F.E. Jensen, and B. Tsao. 1992. Three-dimensional structure of dendritic spines and synapses in rat hippocampus (CA1) at postnatal day 15 and adult ages: implications for the maturation of synaptic physiology and long-term potentiation. *J. Neurosci.* 12:2685–2705.
- Holtmaat, A.J., J.T. Trachtenberg, L. Wilbrecht, G.M. Shepherd, X. Zhang, G.W. Knott, and K. Svoboda. 2005. Transient and persistent dendritic spines in the neocortex in vivo. *Neuron*. 45:279–291.
- Ishii, H., K. Shibuya, Y. Ohta, H. Mukai, S. Uchino, N. Takata, J.A. Rose, and S. Kawato. 2006. Enhancement of nitric oxide production by association of nitric oxide synthase with N-methyl-D-aspartate receptors via postsynaptic density 95 in genetically engineered Chinese hamster ovary cells: real-time fluorescence imaging using nitric oxide sensitive dye. *J. Neurochem.* 96:1531–1539.
- Kasai, H., M. Matsuzaki, J. Noguchi, N. Yasumatsu, and H. Nakahara. 2003. Structure-stability-function relationships of dendritic spines. *Trends Neurosci.* 26:360–368.
- Kim, E., and M. Sheng. 2004. PDZ domain proteins of synapses. *Nat. Rev. Neurosci.* 5:771–781.
- Kim, J.H., D. Liao, L.F. Lau, and R.L. Huganir. 1998. SynGAP: a synaptic RasGAP that associates with the PSD-95/SAP90 protein family. *Neuron*. 20:683–691.
- Knott, G.W., A. Holtmaat, L. Wilbrecht, E. Welker, and K. Svoboda. 2006. Spine growth precedes synapse formation in the adult neocortex in vivo. *Nat. Neurosci.* 9:1117–1124.
- Marrs, G.S., S.H. Green, and M.E. Dailey. 2001. Rapid formation and remodeling of postsynaptic densities in developing dendrites. *Nat. Neurosci.* 4:1006–1013.
- Matsuzaki, M., N. Honkura, G.C. Ellis-Davies, and H. Kasai. 2004. Structural basis of long-term potentiation in single dendritic spines. *Nature*. 429:761–766.
- Migaud, M., P. Charlesworth, M. Dempster, L.C. Webster, A.M. Watabe, M. Makhinson, Y. He, M.F. Ramsay, R.G. Morris, J.H. Morrison, et al. 1998. Enhanced long-term potentiation and impaired learning in mice with mutant postsynaptic density-95 protein. *Nature*. 396:433–439.
- Nikonenko, I., P. Jourdain, and D. Muller. 2003. Presynaptic remodeling contributes to activity-dependent synaptogenesis. *J. Neurosci.* 23:8498–8505.
- Petrak, L.J., K.M. Harris, and S.A. Kirov. 2005. Synaptogenesis on mature hippocampal dendrites occurs via filopodia and immature spines during blocked synaptic transmission. *J. Comp. Neurol.* 484:183–190.
- Popov, V.I., A.A. Deev, O.A. Klimenko, V. Kraev, S.B. Kuz'minykh, N.I. Medvedev, I.V. Patrushev, R.V. Popov, V.V. Rogachevskii, S.S. Khutsiyani, et al. 2005. Three-dimensional reconstruction of synapses and dendritic spines in the rat and ground squirrel hippocampus: new structural-functional paradigms for synaptic function. *Neurosci. Behav. Physiol.* 35:333–341.
- Prange, O., and T.H. Murphy. 2001. Modular transport of postsynaptic density-95 clusters and association with stable spine precursors during early development of cortical neurons. *J. Neurosci.* 21:9325–9333.
- Prange, O., T.P. Wong, K. Gerrow, Y.T. Wang, and A. El-Husseini. 2004. A balance between excitatory and inhibitory synapses is controlled by PSD-95 and neuroligin. *Proc. Natl. Acad. Sci. USA*. 101:13915–13920.
- Schnell, E., M. Sizemore, S. Karimzadeegan, L. Chen, D.S. Bredt, and R.A. Nicoll. 2002. Direct interactions between PSD-95 and stargazin control synaptic AMPA receptor number. *Proc. Natl. Acad. Sci. USA*. 99:13902–13907.
- Stein, V., D.R. House, D.S. Bredt, and R.A. Nicoll. 2003. Postsynaptic density-95 mimics and occludes hippocampal long-term potentiation and enhances long-term depression. *J. Neurosci.* 23:5503–5506.
- Stoppini, L., P.A. Buchs, and D. Muller. 1991. A simple method for organotypic cultures of nervous tissue. *J. Neurosci. Methods*. 37:173–182.
- Sunico, C.R., F. Portillo, D. Gonzalez-Forero, and B. Moreno-Lopez. 2005. Nitric-oxide-directed synaptic remodeling in the adult mammal CNS. *J. Neurosci.* 25:1448–1458.

- Tochio, H., Y.K. Mok, Q. Zhang, H.M. Kan, D.S. Bredt, and M. Zhang. 2000. Formation of nNOS/PSD-95 PDZ dimer requires a preformed beta-finger structure from the nNOS PDZ domain. *J. Mol. Biol.* 303:359–370.
- Toni, N., E.M. Teng, E.A. Bushong, J.B. Aimone, C. Zhao, A. Consiglio, H. van Praag, M.E. Martone, M.H. Ellisman, and F.H. Gage. 2007. Synapse formation on neurons born in the adult hippocampus. *Nat. Neurosci.* 10:727–734.
- Vazquez, L.E., H.J. Chen, I. Sokolova, I. Knuesel, and M.B. Kennedy. 2004. SynGAP regulates spine formation. *J. Neurosci.* 24:8862–8872.
- Vickers, C.A., B. Stephens, J. Bowen, G.W. Arbuthnott, S.G. Grant, and C.A. Ingham. 2006. Neurone specific regulation of dendritic spines in vivo by post synaptic density 95 protein (PSD-95). *Brain Res.* 1090:89–98.
- Xu, W., O.M. Schluter, P. Steiner, B.L. Czervionke, B. Sabatini, and R.C. Malenka. 2008. Molecular dissociation of the role of PSD-95 in regulating synaptic strength and LTD. *Neuron.* 57:248–262.
- Zuo, Y., A. Lin, P. Chang, and W.B. Gan. 2005. Development of long-term dendritic spine stability in diverse regions of cerebral cortex. *Neuron.* 46:181–189.